IEEE Access
Multidisciplinary | Rapid Review | Open Access Journal

Received 21 September 2022, accepted 11 November 2022, date of publication 17 November 2022,
date of current version 22 November 2022.

Digital Object Identifier 10.1109/ACCESS.2022.3223089

RESEARCH ARTICLE

Impact of 3D Antenna Radiation Pattern on Heterogeneous Cellular Networks

MENGXIN ZHOU[1], CHEN CHEN[2], (Member, IEEE), AND XIAOLI CHU[1], (Senior Member, IEEE)

[1]Department of Electronic and Electrical Engineering, The University of Sheffield, S10 2TN Sheffield, U.K.
[2]Department of Electrical Engineering and Electronics, University of Liverpool, L69 3GJ Liverpool, U.K.

Corresponding author: Mengxin Zhou (mzhou15@sheffield.ac.uk)

This work was supported in part by the European Union's Horizon 2020 Research and Innovation Program under the Marie Skłodowska-Curie under Grant 734798.

ABSTRACT Heterogeneous cellular networks (HCNs) play a significant role in 5G networks, but have mainly been modeled and analyzed on a two-dimensional (2D) plane. In this paper, we model a three-dimensional (3D) two-tier HCN consisting of macro-cells and small-cells via a stochastic geometry approach, where the base stations (BSs) in each tier are assigned an appropriate antenna downtilt to enhance the downlink signal and suppress the inter-cell interference. Based on the 3D HCN model, we derive the downlink spatially-averaged coverage probability and area spectral efficiency (ASE) as functions of the BS antenna downtilts, BS heights, BS densities and cell-association bias. To facilitate fast numerical evaluation, we propose accurate approximations for the integral parts in the coverage probability expression. We then obtain the optimal BS antenna downtilts for both tiers that maximize the downlink spatially-averaged coverage probability by using partial derivative and the bisection method. Analytical and simulation results show that for given BS heights, densities of small-cell BSs (SBSs) and cell-association biases of SBSs, our optimized BS antenna downtilts of both tiers can significantly enhance the downlink spatially-averaged coverage probability and ASE in comparison with the fixed BS antenna downtilts network. Useful insights into the 3D deployment of HCNs considering BS antenna downtilts are obtained based on the analytical and simulation results.

INDEX TERMS 3D antenna downtilt, base station height, coverage probability, cell-assciation bias, heterogeneous cellular networks.

I. INTRODUCTION

Heterogeneous cellular network (HCN), which consists of multiple tiers of base stations (BSs), such as macro-cell, pico-cell and femto-cell BSs, is a key technology of the 5th generation (5G) mobile networks [1], [2]. In HCNs, macro-cell BSs (MBSs) typically provide outdoor coverage and support high-speed users, while small-cell BSs (SBSs) provide high capacity to indoor users and outdoor cell-edge users [3]. However, small cells lead to more cell-edge areas, making the aggregate interference environment and the corresponding interference management more complicated in HCNs than in conventional single-tier cellular networks [4].

HCNs have been modeled and analyzed using tools from stochastic geometry on a two-dimensional (2D) plane, where beamforming adjusts only the azimuth angle of a beam while the elevation angle being fixed [5], [6], [7], [8]. However, as the BS density increases and the BS-to-user distances decrease in HCNs, the heights of BSs and users can no longer be ignored [9]. Under a three-dimensional (3D) channel model, 3D beamforming that adjusts the beam angle in both the horizontal and vertical planes can be used to enhance the received signal and mitigate interference by steering a main beam of the BS radiation pattern to an intended user [10], [11].

The associate editor coordinating the review of this manuscript and approving it for publication was Tao Zhou.

In this paper, we investigate the impact of the BS antenna vertical pattern and downtilt on the downlink spatially-averaged coverage probability and area spectral efficiency (ASE) of a two-tier HCN comprising MBSs and SBSs. The optimal BS antenna downtilts of both tiers that maximize the downlink spatially-averaged coverage probability and ASE will be derived. In addition, useful insights into the 3D deployment of BSs in HCNs will be provided based on the analytical and simulation results.

A. RELATED WORKS AND MOTIVATION

Stochastic geometry has been widely explored to evaluate the performance of cellular networks. In [12], the authors analyzed the downlink coverage probability of a single-tier cellular network leveraging stochastic geometry, where the locations of BSs and users were modeled following independent homogeneous Poison point processes (HPPPs). For HCNs, due to the differences in transmit power and BS antenna height between MBSs and SBSs, a bias needs to be added to the received signal of users in the small-cell tier to balance the load between the macro-cell and small-cell tiers in HCNs [13]. The authors in [5] showed that adding a positive bias to the received power from SBSs in an HCN can improve the coverage probability, average ergodic rate, and minimum average user throughput even though the signal-to-noise-plus-interference ratio (SINR) of some cell-edge users decreases. The authors in [14] optimized the cell association bias and traffic offloading fraction to maximize the rate coverage in an HCN. The authors in [15] optimized the cell association bias to maximize the mean downlink SINR in multi-antenna HCNs. In [16], the energy efficiency of a multi-tier HCN was maximized while considering potentially different BS heights and multi-antenna transmission. In [17], the impact of beamforming alignment errors on the coverage probability in a millimeter-wave HCN was investigated under different path loss models, but the BS vertical antenna pattern is not considered, and the antenna gain is assumed to be constant. The authors in [18] analyzed the coverage probability and average user rate with the minimum biased transmission distance scheme in an HCN. In 3D HCNs, as the heights of MBSs are larger than SBSs, the traffic in the small-cell tier is overloaded when adopting the minimum 3D transmission distance-based user association scheme. Therefore, a bias in terms of 3D transmission distance towards users located at the small-cell edge is considered to offload these users to the macro-cell tier [19].

Recently, 3D beamforming has been proposed to improve the performance of HCNs [20], [21], [22]. In [20], a 3D beam selection scheme was proposed to restrain the intra-cell and intercell interference in a downlink multi-cell HCN. In [21], the authors proposed an interference coordination algorithm by leveraging the statistical channel state information and MBS antenna downtilting to balance the ergodic rate and traffic load among different tiers. The authors in [22] simulated the impact of the pico-cell antenna downtilt and vertical beamwidth on the coverage probability and ASE of an HCN leveraging the maximum average SIR user association scheme. The impact of pico-cell BS antenna downtilt, antenna vertical beamwidth, and pico-cell density on the coverage probability and spectral efficiency of a two-tier HCN was investigated in [23], while the impact of the number of dipole antenna elements and SBS antenna downtilt on the ASE and average user rate were studied in [24]. We note that in the aforementioned works, the effect of BS antenna downtilt was studied either via Monte Carlo simulations with a high computational complexity or by numerically solving an intractable optimization problem. The authors in [25] modeled a two-tier HCN using stochastic geometry and maximized the energy efficiency of the HCN by optimizing the MBSs' antenna downtilts for different femto-cell BS densities, but the BS heights and antenna downtilts in the small-cell tier were ignored.

In summary, the existing works have not studied the BS antenna downtilts across all tiers of an HCN, thus missing the opportunity to further enhance the HCN performance, e.g., the downlink coverage probability or ASE, by jointly optimizing the BS antenna downtilts in different tiers.

B. CONTRIBUTIONS

In this paper, we investigate how the BS antenna downtilts of all BSs across different tiers can be jointly optimized to enhance the downlink spatially-averaged coverage probability and ASE in a 3D two-tier HCN composed of MBSs and SBSs, where the locations of multi-antenna MBSs and SBSs follow two independent HPPPs, and the potentially different BS heights and BS radiation patterns are modeled. The main contributions of this work are summarized as follows.

Spatially-averaged coverage probability and ASE analysis for 3D two-tier HCNs: We propose a 3D system model for a two-tier HCN with multi-antenna BSs, where the BS antenna downtilts and BS antenna heights of both tiers are modeled, and each user is served by the BS whose antennas have the shortest biased distance to the user (i.e., the SBS antenna-to-user distance is scaled by a positive bias for cell-association decisions). Assuming that BS antennas in each tier have the same downtilt and height, we derive the expressions for the per-tier association probability, which is the probability that a user is associated with a BS of a certain tier, and the downlink coverage probability of a user conditional on being associated with a certain tier. Based on these two expressions, we obtain the expressions for the downlink spatially-averaged coverage probability and ASE as functions of the BS antenna downtilts, heights and densities for both tiers, and the SBS association bias. Moreover, to facilitate fast numerical evaluation, we propose an accurate approximation for the integral parts in the spatially-averaged coverage probability expression. The accuracy of the derived analytical expressions is assessed by Monte Carlo simulations. The analytical results can provide useful insights into the practical configuration of BS antenna downtilts for both macro-cell and small-cell tiers.

Joint optimization of MBS and SBS antenna downtilts for maximizing the downlink spatially-averaged coverage

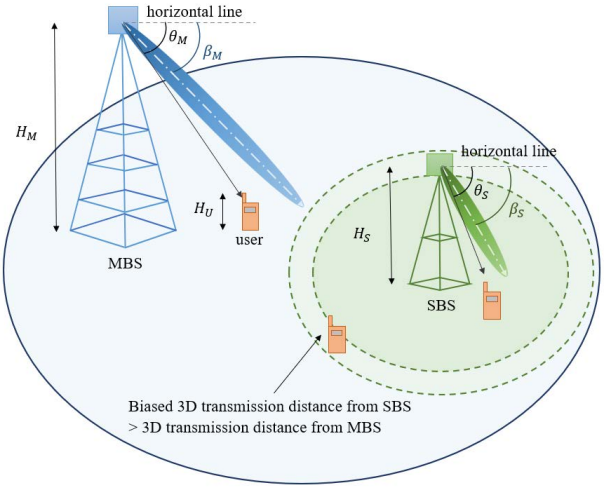

FIGURE 1. A two-tier HCN consisting of MBSs and SBSs with the minimum biased 3D transmission distance user association scheme.

probability: We calculate the optimal pair of MBS and SBS antenna downtilts that maximize the downlink spatially-averaged coverage probability by taking the partial derivative of the derived spatially-averaged coverage probability expression with respect to the MBS (SBS) antenna downtilt, respectively, then letting the partial derivative equal zero and solving the resulting equation for the MBS (SBS) antenna downtilt. The bisection method is used to find the solutions of the partial derivative equations, where we impose a restriction on the MBS (SBS) main beam downtilt values according to the side lobe level and solve the equations iteratively. The solution of each equation is the stationary point of the spatially-averaged coverage probability with respect to the BS antenna downtilt. As the stationary point could be the maximum, the minimum or the saddle point, a second derivative test is proposed to verify the uniqueness and the type of the stationary point to guarantee that the obtained solution corresponds to the maximum coverage probability. The optimal pair of MBS and SBS antenna downtilts are obtained for different SBS heights and densities. The corresponding downlink spatially-averaged coverage probability and ASE are compared to the benchmark schemes that do not consider the BS antenna downtilts.

The reminder of this paper is organized as follows. In Section II, the system model of 3D HCNs is presented. In Section III, the expressions of the downlink spatially-averaged coverage probability and ASE are derived as functions of antenna downtilts of MBSs and SBSs. The method for finding the optimal pair of MBS and SBS antenna downtilts is proposed in Section IV. The numerical and simulation results are presented in Section V. Finally, we conclude this paper in Section VI.

II. SYSTEM MODEL

We consider a two-tier HCN consisting of MBSs and SBSs, as shown in Fig. 1. MBSs and SBSs are distributed on the ground following two independent HPPPs, Φ_M and Φ_S, with densities λ_M and λ_S, respectively. We assume that the BSs of the same tier have the identical transmit power and height, where the MBS transmit power and SBS transmit power are denoted by P_M and P_S, respectively, and the MBS and SBS heights are denoted by H_M and H_S, respectively. Users are distributed in the network area following another independent HPPP Φ_U. Each user has a single antenna with the same height of H_U. We assume that each user is associated with the BS that has the shortest biased transmission distance from the BS antenna to the user antenna, where the SBS antenna-to-user antenna distance is scaled by a positive bias, $B_S > 1$, for use in cell-association decisions. The largest received signal power-based user association scheme may lead to a heavy load for high-power MBSs in a heterogeneous network, while the smallest path loss-based user association scheme ignores the tier-specific user association bias that has been widely considered for load balancing in heterogeneous networks [26]. Additionally, it has been shown in [19] that the shortest biased transmission distance-based user association strategy can achieve the same coverage probability as the largest received signal power-based user association strategy by adjusting the tier-specific user association bias. The largest received signal power association strategy adoption will be investigated in our future work. Each MBS and each SBS have access to all the sub-channels of the network. We assume that each MBS is partitioned into s equal sectors, each covering an azimuth angular spread of $\frac{2\pi}{s}$ and being regarded as a macro-cell. The total number of sub-channels are divided into s orthogonal subsets of equal size, which are allocated to the s sectors of an MBS.

The downlink adopts orthogonal frequency division multiple access (OFDMA) in each cell, hence there is no intra-cell interference. We assume that each link sees independent Rayleigh fading with a unit average power gain. The path loss from MBS i ($i \in \Phi_M$) or SBS j ($j \in \Phi_S$) to a user is given respectively by

$$L_i^M = \left(\left(d_i^M\right)^2 + h_M^2\right)^{-\frac{\alpha_M}{2}}, \tag{1}$$

$$L_j^S = \left(\left(d_j^S\right)^2 + h_S^2\right)^{-\frac{\alpha_S}{2}}, \tag{2}$$

where d_i^M $\left(d_j^S\right)$ is the horizontal distance between a user and MBS i (SBS j); $h_M = H_M - H_U$ and $h_S = H_S - H_U$ denote the height difference between an MBS and a user and that between an SBS and a user, respectively, and are both assumed to be positive; α_M and α_S represent the path loss exponent for the macro-cell and small-cell tiers, respectively.

According to 3GPP [27] and existing works [28], [29], the antenna gain (in dBi) of each antenna equipped at MBS i or SBS j is given respectively by

$$G_i^M = G_{M_h} + G_{M_v}\left(\theta_i^M, \beta_M\right) + G_{M_m}, \tag{3}$$

$$G_j^S = G_{S_h} + G_{S_v}\left(\theta_j^S, \beta_S\right) + G_{S_m}, \tag{4}$$

where G_{M_h} and G_{S_h} are the horizontal gain of an MBS antenna and an SBS antenna, respectively; $G_{M_v}\left(\theta_i^M, \beta_M\right)$ and $G_{S_v}\left(\theta_j^S, \beta_S\right)$ denote the vertical pattern of an antenna at MBS i and SBS j, respectively; $\theta_i^M = \tan^{-1}\left(\frac{h_M}{d_i^M}\right)$ and $\theta_j^S = \tan^{-1}\left(\frac{h_S}{d_j^S}\right)$ are the physical elevation angles of departure (AoD) from MBS i or SBS j to a user, respectively; β_M and β_S are the electrical downtilts of antennas at MBSs and SBSs, respectively; G_{M_m} and G_{S_m} are the maximum antenna gains of MBS and SBS antennas, respectively.

Assuming that each antenna element is a dipole, the vertical pattern of an antenna at MBS i and SBS j can be approximated by [27] and [30]

$$G_{M_v}\left(\theta_i^M, \beta_M\right) = \max\left[-12\left(\frac{\theta_i^M - \beta_M}{\theta_{3dB}}\right)^2, SLL_M\right], \quad (5)$$

$$G_{S_v}\left(\theta_j^S, \beta_S\right) = \max\left[10\log_{10}\left|\cos^{n_S}\left(\theta_j^S - \beta_S\right)\right|, SLL_S\right], \quad (6)$$

where θ_{3dB} is the half-power beamwidth (HPBW) of the MBS antenna radiation pattern; n_S is a parameter determined by the beamwidth of the SBS antenna radiation pattern [30]; SLL_M and SLL_S are the sidelobe levels in the vertical plane of the MBS antenna pattern and the SBS antenna pattern, respectively.

Since the horizontal radiation pattern of antennas is symmetric, sectorizing all MBSs to modify the antenna patterns does not have significant impact on the SIR of the desired user. We assume that the antenna pattern for all BSs are omni-directional in the horizontal plane and the horizontal antenna gain from an MBS antenna equals to that from s sectors with the same sub-channel. Based on this assumption, the effective density of interfering sectors from other MBSs to an MBS user is set as $\frac{\lambda_M}{s}$, and the effective MBS distribution is denoted as an HPPP Φ'_M with density $\frac{\lambda_M}{s}$ [25].

Without loss of generality, we focus on a typical user located at the origin of the 2D ground plane [5], [31]. The signal-to-interference ratio (SIR) of the typical user served by MBS i or SBS j in an arbitrary sub-channel is respectively expressed as

$$\mathrm{SIR}_i^M = \frac{g_i^M P_M L_i^M G_i^M}{I_i^M + I_M^S}, \quad (7)$$

$$\mathrm{SIR}_j^S = \frac{g_j^S P_S L_j^S G_j^S}{I_j^S + I_S^M}, \quad (8)$$

where

$$I_i^M = \sum_{k\in\Phi'_M\setminus\{i\}} g_k^M P_M L_k^M G_k^M,$$

$$I_M^S = \sum_{l\in\Phi_S} g_l^M P_S L_l^M G_l^M,$$

$$I_j^S = \sum_{l\in\Phi_S\setminus\{j\}} g_l^S P_S L_l^S G_l^S,$$

$$I_S^M = \sum_{k\in\Phi'_M} g_k^S P_M L_k^S G_k^S,$$

denote the macro-cell tier interference and small-cell tier interference to the typical user served by MBS i, and the small-cell tier interference and macro-cell tier interference to the typical user served by SBS j, respectively; g_i^M and g_j^S denote the Rayleigh fading power gains of the links from MBS i ($\forall i \in \Phi_M$) and SBS j ($\forall j \in \Phi_S$) to the typical user, respectively, each following an independent and identical exponential distribution exp(1).

III. COVERAGE PROBABILITY AND AREA SPECTRAL EFFICIENCY

In this section, we will derive the downlink coverage probability and ASE as functions of the MBS antenna downtilt and the SBS antenna downtilt for a 3D HCN.

A. TIER ASSOCIATION

The coverage probability averaged over the spatial domain of the two-tier HCN is defined as the probability that the SIR of the typical user is greater than a given threshold τ, and it can be expressed as

$$p_c = \mathcal{P}_M \mathcal{A}_M + \mathcal{P}_S \mathcal{A}_S, \quad (9)$$

where $\mathcal{P}_M$ and $\mathcal{P}_S$ are the spatially-averaged coverage probability conditional on the typical user being associated with an MBS or an SBS, respectively; $\mathcal{A}_M$ and $\mathcal{A}_S$ are the probability that the typical user is associated with an MBS or an SBS, respectively.

Let d_M and d_S denote the horizontal distances from the typical user to the nearest MBS and the nearest SBS, respectively. For use in the cell-association decision making, the biased distance from the closest MBS's antenna or the closest SBS's antenna to the typical user's antenna is written respectively as

$$D_M = \sqrt{d_M^2 + h_M^2}, \quad (10)$$

$$D_S = B_S\sqrt{d_S^2 + h_S^2}. \quad (11)$$

If $D_M < D_S$, then the typical user is associated with the closest MBS; otherwise, the typical user is associated with the closest SBS. Accordingly, the spatially-averaged probability that the typical user is associated with an MBS is expressed as

$$\begin{aligned}\mathcal{A}_M &= \mathbb{E}_{d_M}\left[\Pr\left(D_M < D_S\right)\right] \\ &= \mathbb{E}_{d_M}\left[\Pr\left(d_S^2 > \frac{d_M^2 + h_M^2}{B_S^2} - h_S^2\right)\right]. \end{aligned} \quad (12)$$

Let $\mathcal{R}_M = \frac{d_M^2+h_M^2}{B_S^2} - h_S^2$, then $\Pr\left(D_M < D_S\right) = 1$ if $\mathcal{R}_M \le 0$; if $\mathcal{R}_M > 0$, we have

$$\mathcal{A}_M = \mathbb{E}_{d_M}\left[\Pr\left(d_S > \sqrt{\mathcal{R}_M}\right)\right]$$

$$= \mathbb{E}_{d_M}\left[e^{-\lambda_S \pi \mathcal{R}_M}\right]$$
$$= \int_0^{\gamma_M} f_{d_M}(r)\,\mathrm{d}r + \int_{\gamma_M}^{\infty} e^{-\lambda_S \pi \mathcal{R}_M} f_{d_M}(r)\,\mathrm{d}r$$
$$= 1 - \mathrm{e}^{-\lambda_M \pi \gamma_M^2} + \mathrm{e}^{-\pi\left[\lambda_M \gamma_M^2 + \lambda_S\left(\frac{\gamma_M^2 + h_M^2}{B_S^2} - h_S^2\right)\right]}, \quad (13)$$

where the second line is obtained using the null probability of an HPPP on a 2D plane [5], [12], $f_{d_M}(r) = 2\pi\lambda_M r e^{-\lambda_M \pi r^2}$ is the probability density function (PDF) of d_M [12], and

$$\gamma_M = \begin{cases} \sqrt{h_S^2 B_S^2 - h_M^2}, & \text{if } h_S^2 B_S^2 \geq h_M^2 \\ 0, & \text{if } h_S^2 B_S^2 < h_M^2 \end{cases}. \quad (14)$$

Similarly, the spatially-averaged probability that the typical user is associated with the closest SBS is obtained as

$$\mathcal{A}_S = 1 - \mathrm{e}^{-\lambda_S \pi \gamma_S^2} + \mathrm{e}^{-\pi\left[\lambda_S \gamma_S^2 + \lambda_M\left((\gamma_S^2 + h_S^2)B_S^2 - h_M^2\right)\right]}, \quad (15)$$

where

$$\gamma_S = \begin{cases} \sqrt{\left(\frac{h_M}{B_S}\right)^2 - h_S^2}, & \text{if } \left(\frac{h_M}{B_S}\right)^2 \geq h_S^2 \\ 0, & \text{if } \left(\frac{h_M}{B_S}\right)^2 < h_S^2 \end{cases}. \quad (16)$$

B. COVERAGE PROBABILITY

The spatially-averaged coverage probability conditional on the typical user being associated with an MBS is given by

$$\mathcal{P}_M = \mathbb{E}_{d_i^M}\left[\Pr\left(\mathrm{SIR}_i^M > \tau\right)\right]$$
$$= \int_0^{\infty} \left[\Pr\left(\mathrm{SIR}_i^M > \tau\right)\right] f_{d_i^M}(x)\,\mathrm{d}x$$
$$= \int_0^{\infty} \mathcal{L}_{I_i^M}\mathcal{L}_{I_M^S} f_{d_i^M}(x)\,\mathrm{d}x, \quad (17)$$

where $\mathcal{L}_{I_i^M}$ and $\mathcal{L}_{I_M^S}$ are the Laplace transforms of I_i^M and I_M^S, respectively, and can be calculated by

$$\mathcal{L}_{I_i^M} = \exp\left[-\frac{2\pi\lambda_M}{s}\int_x^{\infty} \frac{d_k^M}{1 + \mathcal{K}_i^M \frac{G_i^M}{G_k^M}}\mathrm{d}d_k^M\right] \quad (18)$$

$$\mathcal{L}_{I_M^S} = \exp\left[-2\pi\lambda_S \int_{W_M}^{\infty} \frac{d_l^M}{1 + \mathcal{K}_M^S \frac{G_i^M}{G_l^M}}\mathrm{d}d_l^M\right], \quad (19)$$

where $\mathcal{K}_i^M = \frac{L_i^M}{\tau L_k^M}$ and $\mathcal{K}_M^S = \frac{P_M L_i^M}{\tau P_S L_l^M}$; W_M is the minimum horizontal distance from the typical user to an interfering MBS and is given by

$$W_M = \begin{cases} \sqrt{\frac{x^2 + h_M^2}{B_S^2} - h_S^2}, & \text{if } x \geq \gamma_M \\ 0, & \text{if } x < \gamma_M \end{cases}. \quad (20)$$

In addition, the PDF of d_i^M is expressed as

$$f_{d_i^M}(x) = \begin{cases} \frac{2\pi\lambda_M}{\mathcal{A}_M} x e^{-\lambda_M \pi x^2}, & \text{if } x < \gamma_M \\ \frac{2\pi\lambda_M}{\mathcal{A}_M} x e^{-\pi\left[x^2\left(\lambda_M + \frac{\lambda_S}{B_S^2}\right) + Z_M\right]}, & \text{if } x \geq \gamma_M \end{cases}, \quad (21)$$

where $Z_M = \lambda_S\left(\left(\frac{h_M}{B_S}\right)^2 - h_S^2\right)$.

Proof: See Appendix A.

Similarly, the spatially-averaged coverage probability conditional on the typical user being associated with an SBS is obtained as

$$\mathcal{P}_S = \mathbb{E}_{d_j^S}\left[\Pr\left(\mathrm{SIR}_j^S > \tau\right)\right]$$
$$= \int_0^{\infty} \left[\Pr\left(\mathrm{SIR}_j^S > \tau\right)\right] f_{d_j^S}(y)\,\mathrm{d}y$$
$$= \int_0^{\infty} \mathcal{L}_{I_j^S}\mathcal{L}_{I_S^M} f_{d_j^S}(y)\,\mathrm{d}y. \quad (22)$$

where $\mathcal{L}_{I_j^S}$ and $\mathcal{L}_{I_S^M}$ are the Laplace transforms of I_j^S and I_M^S, respectively, and can be calculated by

$$\mathcal{L}_{I_j^S} = \exp\left[-2\pi\lambda_S \int_y^{\infty} \frac{d_l^S}{1 + \mathcal{K}_j^S \frac{G_j^S}{G_l^S}}\mathrm{d}d_l^S\right] \quad (23)$$

$$\mathcal{L}_{I_S^M} = \exp\left[\frac{-2\pi\lambda_M}{s}\int_{W_S}^{\infty} \frac{d_k^S}{1 + \mathcal{K}_S^M \frac{G_j^M}{G_k^S}}\mathrm{d}d_k^S\right], \quad (24)$$

where $\mathcal{K}_j^S = \frac{L_j^S}{\tau L_l^S}$ and $\mathcal{K}_S^M = \frac{P_S L_j^S}{\tau P_M L_k^S}$; W_S is the minimum horizontal distance from the typical user to an interfering SBS and is given by

$$W_S = \begin{cases} \sqrt{\left(y^2 + h_S^2\right)B_S^2 - h_M^2}, & \text{if } y \geq \gamma_S \\ 0, & \text{if } y < \gamma_S \end{cases}. \quad (25)$$

In addition, the PDF of d_j^S is expressed as

$$f_{d_j^S}(y) = \begin{cases} \frac{2\pi\lambda_S}{\mathcal{A}_S} y e^{-\lambda_S \pi y^2}, & \text{if } y < \gamma_S \\ \frac{2\pi\lambda_S}{\mathcal{A}_S} y e^{-\pi\left[y^2\left(\lambda_S + \lambda_M B_S^2\right) + Z_S\right]}, & \text{if } y \geq \gamma_S \end{cases}, \quad (26)$$

where $Z_S = \lambda_M\left(h_S^2 B_S^2 - h_M^2\right)$.

To simplify the numerical calculation for the conditional spatially-averaged coverage probabilities, we leverage the Gaussian quadrature method to approximate the integral parts [33]. Letting $\mathcal{F}(x) = \mathcal{L}_{I_i^M}\mathcal{L}_{I_M^S} f_{d_i^M}(x)$, (17) can be approximated by

$$\mathcal{P}_M = \int_0^{\infty} \mathcal{F}(x)\mathrm{d}x$$
$$\overset{(a)}{=} \frac{\zeta}{2}\int_{-1}^{1} \mathcal{F}\left(\frac{\zeta}{2}\omega + \frac{\zeta}{2}\right)\mathrm{d}\omega$$

$$= \frac{\zeta}{2}\int_{-1}^{1}\frac{\mathcal{F}\left(\frac{\zeta}{2}\omega+\frac{\zeta}{2}\right)\sqrt{1-\omega^2}}{\sqrt{1-\omega^2}}\mathrm{d}\omega$$
$$\overset{(b)}{\approx} \frac{\zeta\pi}{2Q}\left[\sum_{q=1}^{Q}\mathcal{F}\left(\frac{\zeta}{2}\omega_q+\frac{\zeta}{2}\right)\sqrt{1-\omega_q^2}\right], \quad (27)$$

where $\zeta \to \infty$ denotes the largest possible distance from the typical user, $\omega_q = \frac{2}{\zeta}\cos\left(\frac{2q-1}{2Q}\pi\right) - 1$, $q = 1, \ldots, Q$, and Q is the sample size, which determines the accuracy of this approximation, (a) is obtained by substituting $x = \frac{\zeta}{2}\omega + \frac{\zeta}{2}$ into the integral of the first line, and (b) follows from Chebyshev–Gauss quadrature [33].

Letting $\mathcal{G}\left(d_k^M\right) = \frac{d_k^M}{1+\left(\mathcal{K}_M P_M L_k^M G_k^M\right)^{-1}}$, $\mathcal{H}\left(d_l^M\right) = \frac{d_l^M}{1+\left(\mathcal{K}_M P_S L_l^M G_l^M\right)^{-1}}$, (18) and (19) can be written as

$$\begin{aligned}\mathcal{L}_{I_i^M} &= \exp\left[\frac{-2\pi\lambda_M}{s}\int_x^{\zeta}\mathcal{G}\left(d_k^M\right)\mathrm{d}d_k^M\right]\\ &= \exp\left[\frac{-\pi\lambda_M}{s}(\zeta-x)\right.\\ &\quad\left.\times\int_{-1}^{1}\mathcal{G}\left(\frac{\zeta-x}{2}u_M+\frac{\zeta+x}{2}\right)\mathrm{d}u_M\right] \quad (28)\\ &= \exp\left\{\frac{-\pi^2\lambda_M}{sC}(\zeta-x)\times\right.\\ &\quad\left.\sum_{c=1}^{C}\left[\mathcal{G}\left(\frac{\zeta-x}{2}u_c^C+\frac{\zeta+x}{2}\right)\sqrt{1-\left(u_c^C\right)^2}\right]\right\},\end{aligned}$$

$$\begin{aligned}\mathcal{L}_{I_M^S} &= \exp\left[-2\pi\lambda_S\int_{W_M}^{\zeta}\mathcal{H}\left(d_l^M\right)\mathrm{d}d_l^M\right]\\ &= \exp\left[-\pi\lambda_S(\zeta-W_M)\right.\\ &\quad\left.\times\int_{-1}^{1}\mathcal{H}\left(\frac{\zeta-W_M}{2}v_M+\frac{\zeta+W_M}{2}\right)\mathrm{d}v_M\right]\\ &= \exp\left\{\frac{-\pi^2\lambda_S}{N}(\zeta-W_M)\times\right.\\ &\quad\left.\sum_{o=1}^{O}\left[\mathcal{H}\left(\frac{\zeta-W_M}{2}v_o^O+\frac{\zeta+W_M}{2}\right)\sqrt{1-\left(v_o^O\right)^2}\right]\right\},\end{aligned} \quad (29)$$

where $u_c^C = \frac{2}{\zeta-x}\cos\left(\frac{2c-1}{2C}\pi\right) - \frac{\zeta+x}{\zeta-x}$, $c = 1, \ldots, C$, and C is the sample size; $v_o^O = \frac{2}{\zeta-W_M}\cos\left(\frac{2o-1}{2O}\pi\right) - \frac{\zeta+W_M}{\zeta-W_M}$, $o = 1, \ldots, O$, and O is the sample size.

The approximation of $\mathcal{P}_S$ can be derived following the same steps.

C. AREA SPECTRAL EFFICIENCY

The ASE evaluates the spectral efficiency of the two-tier HCN per unit area [34] (in bps/Hz/km^2) and is given by [35]

$$ASE = \left(\lambda_M\mathcal{P}_M\mathcal{A}_M + \lambda_S\mathcal{P}_S\mathcal{A}_S\right)\log_2(1+\tau). \quad (30)$$

IV. THE OPTIMAL ANTENNA DOWNTILT PAIR

In this section, we maximize the spatially-averaged coverage probability by optimizing the the electrical downtilts of antennas at MBSs and SBSs, i.e., β_M and β_S, and formulate the optimization problem as

$$\begin{aligned}\max_{\beta_M,\beta_S}\quad & p_c\\ \text{s.t.}\quad & 0 \le \beta_M \le \frac{\pi}{2},\\ & 0 \le \beta_S \le \frac{\pi}{2}.\end{aligned} \quad (31)$$

This problem can be addressed via calculating the partial derivative of the spatially-averaged coverage probability with respect to the independent variable β_M and β_S, respectively [36]. The maximum point $\left(\beta_M^*, \beta_S^*\right)$ is one of the stationary points of $p_c\left(\beta_M, \beta_S\right)$ by working out $\frac{\partial p_c}{\partial\beta_M}$ and $\frac{\partial p_c}{\partial\beta_S}$ and setting both to zero. According to (9), variables β_M and β_S only have impact on $\mathcal{P}_M$ and $\mathcal{P}_S$. Therefore, the optimal BS antenna downtilt pair is obtained from the following equations:

$$\begin{aligned}\left\{\beta_M^*, \beta_S^*\right\} = &\left\{\arg_{\beta_M}\left\{\mathcal{A}_M\frac{\partial\mathcal{P}_M}{\partial\beta_M}+\mathcal{A}_S\frac{\partial\mathcal{P}_S}{\partial\beta_M}=0\right\},\right.\\ &\left.\arg_{\beta_S}\left\{\mathcal{A}_M\frac{\partial\mathcal{P}_M}{\partial\beta_S}+\mathcal{A}_S\frac{\partial\mathcal{P}_S}{\partial\beta_S}=0\right\}\right\},\end{aligned} \quad (32)$$

where

$$\begin{aligned}\frac{\partial\mathcal{P}_M}{\partial\beta_M} &= \int_0^{\infty}\left[\frac{\partial}{\partial\beta_M}\mathcal{L}_{I_i^M}\mathcal{L}_{I_M^S}\right]f_{d_i^M}(x)\,\mathrm{d}x\\ &= \int_0^{\infty}\left[\mathcal{L}_{I_i^M}\mathcal{L}_{I_M^S}\left(\mathcal{L}'_{I_i^M|\beta_M}+\mathcal{L}'_{I_M^S|\beta_M}\right)\right]f_{d_i^M}(x)\,\mathrm{d}x, \quad (33)\\ \frac{\partial\mathcal{P}_S}{\partial\beta_M} &= \int_0^{\infty}\left[\frac{\partial}{\partial\beta_M}\mathcal{L}_{I_j^S}\mathcal{L}_{I_S^M}\right]f_{d_j^S}(y)\,\mathrm{d}y\\ &= \int_0^{\infty}\left[\mathcal{L}_{I_j^S}\mathcal{L}_{I_S^M}\mathcal{L}'_{I_S^M|\beta_M}\right]f_{d_j^S}(y)\,\mathrm{d}y, \quad (34)\\ \frac{\partial\mathcal{P}_M}{\partial\beta_S} &= \int_0^{\infty}\left[\frac{\partial}{\partial\beta_S}\mathcal{L}_{I_i^M}\mathcal{L}_{I_M^S}\right]f_{d_i^M}(x)\,\mathrm{d}x\\ &= \int_0^{\infty}\left[\mathcal{L}_{I_i^M}\mathcal{L}_{I_M^S}\mathcal{L}'_{I_M^S|\beta_S}\right]f_{d_i^M}(x)\,\mathrm{d}x, \quad (35)\\ \frac{\partial\mathcal{P}_S}{\partial\beta_S} &= \int_0^{\infty}\left[\frac{\partial}{\partial\beta_S}\mathcal{L}_{I_j^S}\mathcal{L}_{I_S^M}\right]f_{d_j^S}(y)\,\mathrm{d}y\\ &= \int_0^{\infty}\left[\mathcal{L}_{I_j^S}\mathcal{L}_{I_S^M}\left(\mathcal{L}'_{I_j^S|\beta_S}+\mathcal{L}'_{I_S^M|\beta_S}\right)\right]f_{d_j^S}(y)\,\mathrm{d}y. \quad (36)\end{aligned}$$

Here we define

$$\mathcal{L}'_{I_i^M|\beta_M} = -\frac{2\pi\lambda_M}{s}\int_x^{\infty}\left[d_k^M\mathcal{K}_i^M\frac{G_i^M\frac{\partial G_k^M}{\partial\beta_M}-\frac{\partial G_i^M}{\partial\beta_M}G_k^M}{\left(G_k^M+\mathcal{K}_i^M G_i^M\right)^2}\right]\mathrm{d}d_k^M, \quad (37)$$

$$\mathcal{L}'_{I_M^S|\beta_M} = -2\pi\lambda_S \int_{W_M}^{\infty} \left[-d_l^M \mathcal{K}_M^S \frac{\frac{\partial G_i^M}{\partial \beta_M}}{G_l^M \left(1 + \mathcal{K}_M^S \frac{G_i^M}{G_l^M}\right)^2} \right] \mathrm{d}d_l^M, \quad (38)$$

$$\mathcal{L}'_{I_S^M|\beta_M} = -\frac{2\pi\lambda_M}{s} \int_{W_S}^{\infty} \left[d_k^S \mathcal{K}_S^M G_j^S \frac{\frac{\partial G_k^S}{\partial \beta_M}}{\left(G_k^S + \mathcal{K}_S^M G_j^S\right)^2} \right] \mathrm{d}d_k^S, \quad (39)$$

$$\mathcal{L}'_{I_M^S|\beta_S} = -2\pi\lambda_S \int_{W_M}^{\infty} \left[d_l^M \mathcal{K}_M^S G_i^M \frac{\frac{\partial G_l^M}{\partial \beta_S}}{\left(G_l^M + \mathcal{K}_M^S G_i^M\right)^2} \right] \mathrm{d}d_l^M, \quad (40)$$

$$\mathcal{L}'_{I_j^S|\beta_S} = -2\pi\lambda_S \int_{y}^{\infty} \left[d_l^S \mathcal{K}_j^S \frac{G_j^S \frac{\partial G_l^S}{\partial \beta_S} - \frac{\partial G_j^S}{\partial \beta_S} G_l^S}{\left(G_l^S + \mathcal{K}_j^S G_j^S\right)^2} \right] \mathrm{d}d_l^S, \quad (41)$$

$$\mathcal{L}'_{I_S^M|\beta_S} = -\frac{2\pi\lambda_M}{s} \int_{W_S}^{\infty} \left[-d_k^S \mathcal{K}_S^M \frac{\frac{\partial G_j^S}{\partial \beta_S}}{G_k^S \left(1 + \mathcal{K}_S^M \frac{G_j^S}{G_k^S}\right)^2} \right] \mathrm{d}d_k^S. \quad (42)$$

Since β_S is in the range of $\left[0, \frac{\pi}{2}\right]$, $\cos^{n_S}\left(\beta_S - \theta_j^S\right)$ in (6) is always non-negative. The derivative of the antenna main lobe pattern with respect to β_M and β_S from MBS i and SBS j are computed as

$$\frac{\partial G_i^M}{\partial \beta_M} = \frac{2.4 \log 10 G_{M_m}}{\theta_{3dB}^2} 10^{-1.2\left(\frac{\theta_i^M - \beta_M}{\theta_{3dB}}\right)^2} \left(\theta_i^M - \beta_M\right), \quad (43)$$

$$\frac{\partial G_j^S}{\partial \beta_S} = n_S G_{S_m} \cos^{n_S - 1}\left(\theta_j^S - \beta_S\right) \sin\left(\theta_j^S - \beta_S\right). \quad (44)$$

In order to verify the uniqueness of the stationary point which is derived from differential equations in (32), we solve them separately by holding the invariable downtilt of each equation in the range of $\left[0, \frac{\pi}{2}\right]$. We reduce the complexity of the calculation in (32) by a bisection method, which is shown in Algorithm 1, where $\mu, \mu' \in \{M, S\}$ indicates whether the serving BS is an MBS or an SBS. If $\mu = M$, $\mu' = S$; If $\mu = S$, $\mu' = M$. The range of the optimal MBS antenna downtilt and the optimal SBS antenna downtilt are restricted as $\beta_M^* \in \left[\beta_M^{\min}, \beta_M^{\max}\right]$ and $\beta_S^* \in \left[\beta_S^{\min}, \beta_S^{\max}\right]$, respectively. According to (5) and (6), the bounds of β_μ are calculated as follows:

$$-12\left(\frac{\tan^{-1}\left(\frac{h_M}{x}\right) - \beta_M}{\theta_{3dB}}\right)^2 \geq SLL_M, \quad (45)$$

$$10\log_{10}\left|\cos^{n_S}\left(\tan^{-1}\left(\frac{h_S}{y}\right) - \beta_S\right)\right| \geq SLL_S. \quad (46)$$

Combining these bounds with (31) gives

$$\begin{aligned}
\beta_M^{\min} &= \max\left[\tan^{-1}\left(\frac{h_M}{x_{max}}\right) - \theta_{3dB}\sqrt{\frac{SLL_M}{12}}, 0\right], \\
\beta_M^{\max} &= \min\left[\tan^{-1}\left(\frac{h_M}{x_{min}}\right) + \theta_{3dB}\sqrt{\frac{SLL_M}{12}}, \frac{\pi}{2}\right], \quad (47) \\
\beta_S^{\min} &= \max\left[\tan^{-1}\left(\frac{h_S}{y_{max}}\right) - \cos^{-1}\left(\sqrt[n_S]{SLL_S}\right), 0\right], \\
\beta_S^{\max} &= \min\left[\tan^{-1}\left(\frac{h_S}{y_{min}}\right) + \cos^{-1}\left(\sqrt[n_S]{SLL_S}\right), \frac{\pi}{2}\right],
\end{aligned} \quad (48)$$

where x_{min} and x_{max} (y_{min} and y_{max}) are constraints of the horizontal distance from a typical MBS (SBS) user to its serving BS. According to (21) and (26), for a given probability σ, the constraints of the distance are obtained by $Pr(x_{min} \leq x \leq x_{max}) = f_{d_i^M}(x) \geq \sigma$ and $Pr(y_{min} \leq y \leq y_{max}) = f_{d_j^S}(y) \geq \sigma$.

Algorithm 1 Bisection method.

1. Initialize $\beta_\mu^{\text{lower}} = \beta_\mu^{\min}$ and $\beta_\mu^{\text{upper}} = \beta_\mu^{\max}$.
   Calculate $p'_{c_{min}} = \mathcal{A}_M \frac{\partial \mathcal{P}_\mu\left(\beta_\mu^{\min}\right)}{\partial \beta_\mu^{\min}} + \mathcal{A}_S \frac{\partial \mathcal{P}_{\mu'}\left(\beta_\mu^{\min}\right)}{\partial \beta_\mu^{\min}}$.
2. Calculate p'_c for $\beta_\mu = \frac{\beta_\mu^{\text{lower}} + \beta_\mu^{\text{upper}}}{2}$.
3. If $p'_{c_{min}} p'_c > 0$, then set $\beta_\mu^{\text{lower}} = \beta_\mu, p'_{c_{min}} = p'_c$.
   Otherwise, set $\beta_\mu^{\text{upper}} = \beta_\mu$.
4. Stop when $\left|\beta_\mu^{\text{upper}} - \beta_\mu^{\text{lower}}\right|$ is less than a predefined value.

To prove the stationary point is a local maximum point, we employ the second derivative test to classify the type of this point [37]. The second derivative of p_c with respect to β_M and β_S are derived from (33), (34), (35) and (36) as

$$\begin{aligned}
\frac{\partial^2 p_c}{\partial \beta_M^2} &= \mathcal{A}_M \frac{\partial^2 \mathcal{P}_M}{\partial \beta_M^2} + \mathcal{A}_S \frac{\partial^2 \mathcal{P}_S}{\partial \beta_M^2} \\
&= \int_0^{\infty} \left[\frac{\partial^2}{\partial \beta_M^2} \mathcal{L}_{I_i^M} \mathcal{L}_{I_M^S}\right] f_{d_i^M}(x)\mathrm{d}x \\
&\quad + \int_0^{\infty} \left[\frac{\partial^2}{\partial \beta_M^2} \mathcal{L}_{I_j^S} \mathcal{L}_{I_S^M}\right] f_{d_j^S}(y)\mathrm{d}y \\
&= \int_0^{\infty} \left[\mathcal{L}_{I_i^M} \mathcal{L}_{I_M^S} \left[\left(\mathcal{L}'_{I_i^M|\beta_M} + \mathcal{L}'_{I_M^S|\beta_M}\right)^2 \right.\right. \\
&\quad \left.\left. + \left(\mathcal{L}''_{I_i^M|\beta_M} + \mathcal{L}''_{I_M^S|\beta_M}\right)\right]\right] f_{d_i^M}(x)\,\mathrm{d}x
\end{aligned}$$

$$= \int_0^{\infty} \left[\mathcal{L}_{I_j^S} \mathcal{L}_{I_S^M} \left[\left(\mathcal{L}'_{I_S^M|\beta_M} \right)^2 + \mathcal{L}''_{I_S^M|\beta_M} \right] \right] f_{d_j^S}(y) \mathrm{d}y, \tag{49}$$

$$\frac{\partial^2 p_c}{\partial \beta_S^2} = \mathcal{A}_M \frac{\partial^2 \mathcal{P}_M}{\partial \beta_S^2} + \mathcal{A}_S \frac{\partial^2 \mathcal{P}_S}{\partial \beta_S^2}$$
$$= \int_0^{\infty} \left[\frac{\partial^2}{\partial \beta_S^2} \mathcal{L}_{I_i^M} \mathcal{L}_{I_M^S} \right] f_{d_i^M}(x) \mathrm{d}x + \int_0^{\infty} \left[\frac{\partial^2}{\partial \beta_S^2} \mathcal{L}_{I_j^S} \mathcal{L}_{I_S^M} \right] f_{d_j^S}(y) \mathrm{d}y$$
$$= \int_0^{\infty} \left[\mathcal{L}_{I_i^M} \mathcal{L}_{I_M^S} \left[\left(\mathcal{L}'_{I_M^S|\beta_S} \right)^2 + \mathcal{L}''_{I_M^S|\beta_S} \right] \right] f_{d_i^M}(x) \mathrm{d}x$$
$$= \int_0^{\infty} \left[\mathcal{L}_{I_j^S} \mathcal{L}_{I_S^M} \left[\left(\mathcal{L}'_{I_j^S|\beta_S} + \mathcal{L}'_{I_S^M|\beta_S} \right)^2 + \left(\mathcal{L}''_{I_j^S|\beta_S} + \mathcal{L}''_{I_S^M|\beta_S} \right) \right] \right] f_{d_j^S}(y) \, \mathrm{d}y, \tag{50}$$

where

$$\mathcal{L}''_{I_i^M|\beta_M} = -\frac{2\pi\lambda_M}{s} \int_x^{\infty} d_k^M \mathcal{K}_i^M \times \left[\frac{\left(G_i^M \frac{\partial^2 G_k^M}{\partial \beta_M^2} - G_k^M \frac{\partial^2 G_i^M}{\partial \beta_M^2} \right) \left(G_k^M + \mathcal{K}_i^M G_i^M \right)}{\left(G_k^M + \mathcal{K}_i^M G_i^M \right)^3} - \frac{2 \left(\frac{\partial G_k^M}{\partial \beta_M} + \mathcal{K}_i^M \frac{\partial G_i^M}{\partial \beta_M} \right) \left(G_i^M \frac{\partial G_k^M}{\partial \beta_M} - G_k^M \frac{\partial G_i^M}{\partial \beta_M} \right)}{\left(G_k^M + \mathcal{K}_i^M G_i^M \right)^3} \right] \mathrm{d}d_k^M, \tag{51}$$

$$\mathcal{L}''_{I_M^S|\beta_M} = -2\pi\lambda_S \int_{W_M}^{\infty} -d_l^M \mathcal{K}_M^S \times \frac{\frac{\partial^2 G_i^M}{\partial \beta_M^2} \left(1 + \mathcal{K}_M^S \frac{G_i^M}{G_l^M} \right) - \frac{2\mathcal{K}_M^S}{G_l^M} \left(\frac{\partial G_i^M}{\partial \beta_M} \right)^2}{G_l^M \left(1 + \mathcal{K}_M^S \frac{G_i^M}{G_l^M} \right)^3} \mathrm{d}d_k^S, \tag{52}$$

$$\mathcal{L}''_{I_S^M|\beta_M} = -\frac{2\pi\lambda_M}{s} \int_{W_S}^{\infty} d_k^S \mathcal{K}_S^M G_j^S \times \frac{\frac{\partial^2 G_k^S}{\partial \beta_M^2} \left(G_k^S + \mathcal{K}_S^M G_j^S \right) - 2 \left(\frac{\partial G_k^S}{\partial \beta_M} \right)^2}{\left(G_k^S + \mathcal{K}_S^M G_j^S \right)^3} \mathrm{d}d_k^S, \tag{53}$$

$$\mathcal{L}''_{I_M^S|\beta_S} = -2\pi\lambda_S \int_{W_M}^{\infty} d_l^M \mathcal{K}_M^S G_i^M \times \frac{\frac{\partial^2 G_l^M}{\partial \beta_S^2} \left(G_l^M + \mathcal{K}_M^S G_i^M \right) - 2 \left(\frac{\partial G_l^M}{\partial \beta_S} \right)^2}{\left(G_l^M + \mathcal{K}_M^S G_i^M \right)^3} \mathrm{d}d_l^M \tag{54}$$

$$\mathcal{L}''_{I_j^S|\beta_S} = -2\pi\lambda_S \int_y^{\infty} d_l^S \mathcal{K}_j^S \times \left[\frac{\left(G_j^S \frac{\partial^2 G_l^S}{\partial \beta_S^2} - G_l^S \frac{\partial^2 G_j^S}{\partial \beta_S^2} \right) \left(G_l^S + \mathcal{K}_j^S G_j^S \right)}{\left(G_l^S + \mathcal{K}_j^S G_j^S \right)^3} - \frac{2 \left(\frac{\partial G_l^S}{\partial \beta_S} + \mathcal{K}_j^S \frac{\partial G_j^S}{\partial \beta_S} \right) \left(G_j^S \frac{\partial G_l^S}{\partial \beta_S} - G_l^S \frac{\partial G_j^S}{\partial \beta_S} \right)}{\left(G_l^S + \mathcal{K}_j^S G_j^S \right)^3} \right] \mathrm{d}d_l^S, \tag{55}$$

$$\mathcal{L}''_{I_S^M|\beta_S} = -\frac{2\pi\lambda_M}{s} \int_{W_S}^{\infty} -d_k^S \mathcal{K}_S^M \times \frac{\frac{\partial^2 G_j^S}{\partial \beta_S^2} \left(1 + \mathcal{K}_S^M \frac{G_j^S}{G_k^S} \right) - \frac{2\mathcal{K}_S^M}{G_k^S} \left(\frac{\partial G_j^S}{\partial \beta_S} \right)^2}{G_k^S \left(1 + \mathcal{K}_S^M \frac{G_j^S}{G_k^S} \right)^3} \mathrm{d}d_l^M. \tag{56}$$

From (43) and (44), the second derivative of the antenna main lobe pattern with respect to β_M and β_S from MBS i and SBS j are

$$\frac{\partial^2 G_i^M}{\partial \beta_M^2} = \frac{2.4 \log 10 G_{M_m}}{\theta_{3dB}^2} 10^{-1.2\left(\frac{\theta_i^M - \beta_M}{\theta_{3dB}}\right)^2} \left[\left(\frac{\theta_i^M - \beta_M}{\theta_{3dB}} \right)^2 - 1 \right], \tag{57}$$

$$\frac{\partial^2 G_j^S}{\partial \beta_S^2} = n_S G_{S_m} \cos^{n_S} \left(\theta_j^S - \beta_S \right) \left[(n_S - 1) \tan^2 \left(\theta_j^S - \beta_S \right) - 1 \right]. \tag{58}$$

If $\frac{\partial^2 p_c}{\partial \beta_\mu^2} < 0$, then the stationary point is a local maximum point; if $\frac{\partial^2 p_c}{\partial \beta_\mu^2} > 0$, then the stationary point is a local minimum point; If $\frac{\partial^2 p_c}{\partial \beta_\mu^2} = 0$, then the stationary point can be any type and determined by gradients at both sides of it.

TABLE 1. Simulation settings.

	Parameter	Value
Basic Simulation Parameters	Density of MBSs,λ_M	10 BS/km^2
	Density of SBSs,λ_M	2×10^2 BS/km^2
	Transmit power of MBSs,P_M	48 dBm
	Transmit power of SBSs,P_S	33 dBm
	Height of MBSs, H_M	20 m
	Height of SBSs, H_S	6 m
	Height of users, H_U	1 m
	Path loss exponent of macro-cell tier, α_M	3.8
	Path loss exponent of small-cell tier, α_S	4
	Coverage probability threshold, τ	0 dB
	Number of macro-cell sectors, s	3
MBS Antenna Parameters	Vertical HPBW of MBSs, θ_{3dB}	$\frac{\pi}{6}$ rad
	Vertical sidelobe level of MBSs, SLL_M	-20 dB
	Maximum antenna gain of MBSs, G_{M_m}	18 dBi
SBS Antenna Parameters	number of elements n_S	4 47.64
	Vertical sidelobe level of SBSs, SLL_S	-12 dB
	Maximum antenna gain of SBSs, G_{S_m}	8.15 dBi

V. NUMERICAL RESULTS

In this section, we present the results of the analytical expressions to evaluate the performance of the proposed 3D two-tier HCNs, and investigate the impact of the BS antenna downtilts. The maximum spatially-averaged coverage probability and ASE are obtained with the optimal MBS antenna downtilt and SBS antenna downtilt.

A. VERIFICATION OF SYSTEM MODEL ANALYSIS

We first compare results of the spatially-averaged coverage probability for different number of SBS antenna elements from numerical analysis and Monte-Carlo simulations to verify the accuracy of deductions and approximation methods. Each Monte-Carlo simulation is performed with 2×10^4 independent random realizations. In each realization, assuming that a typical user is located at the origin on a 2D ground plane, we simulate an HCN following the system model defined in Section II in a circular region centered at the origin with a radius of 3000 m. Unless otherwise specified, the simulation parameters are set in Table 1.

In Fig. 2, the spatially-averaged coverage probabilities for different SBS antenna elements with no biasing of small cell are depicted in analysis and simulation, respectively. The antenna downtilt for macro-cell tier is set at $\frac{\pi}{4}$ rad. According to [24], for 1-element dipole antenna, $n_S = 2.75$, SLL_S is not required, $G_{S_m} = 2.15$ dBi; for 2-element dipole antenna, $n_S = 11.73$, $SLL_S = 10$ dB, $G_{S_m} = 5.15$ dBi. It can be seen that analytical results match simulation results very well, which attests to the accuracy of derivations and the approximation method in Section III. In addition, comparing curves for different number of SBS dipole elements, we observe that the SBS antenna downtilt angles increase first then decrease as beams tilt down. The BS antenna with more elements leads to a larger maximum coverage probability. In general, the gain

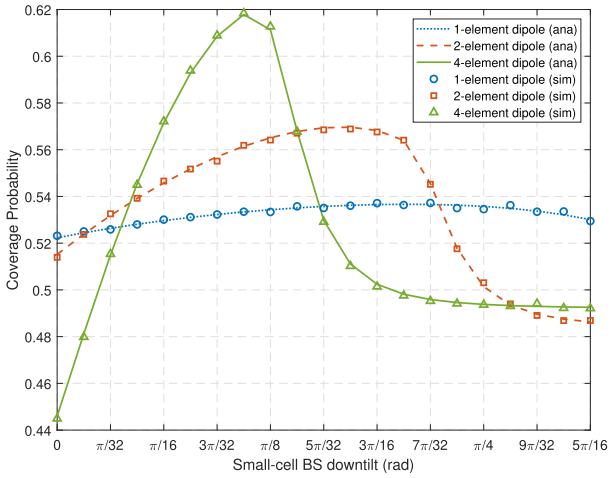

FIGURE 2. Spatially-averaged coverage probability of a two-tier HCN versus the SBS antenna downtilt for different number of SBS antenna elements in analysis and simulation, respectively.

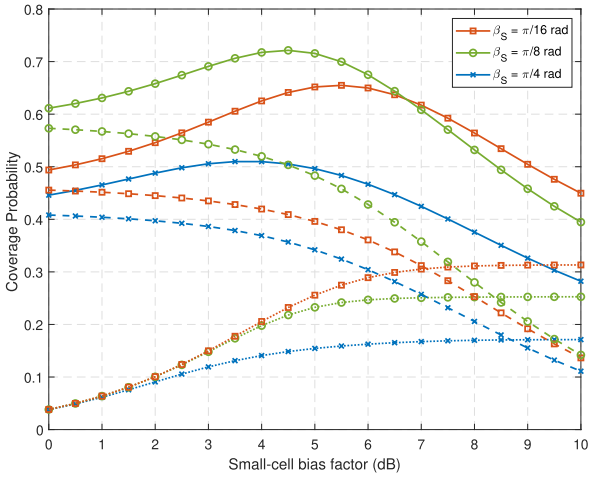

FIGURE 3. Spatially-averaged coverage probability versus the small-cell association bias in the macro-cell tier (dotted lines), small-cell tier (dashed lines), and whole HCN (solid lines) for different SBS antenna downtilts at $\beta_M = \frac{\pi}{4}$ rad.

of the antenna element with a narrow vertical beamwidth is larger than that with a wide vertical beamwidth. The coverage probability for the 4-element antenna changes rapidly due to the small coverage for the narrow beam. Additionally, the optimal SBS antenna downtilt for the 4-element dipole antenna is smaller than that for other number of antennas because cell edge users cannot receive adequate desired signals when their associated SBSs provide large tilting beams.

B. IMPACT OF MBS AND SBS ANTENNA DOWNTILTS, SBS BIASING, HEIGHT AND DENSITY

The numerical results of spatially-averaged coverage probability and ASE with respect to the MBS antenna downtilt, SBS antenna downtilt, SBS biasing, SBS height and SBS density are obtained in this subsection.

Fig. 3 illustrates the spatially-averaged coverage probability of macro-cell tier, small-cell tier and the whole HCN

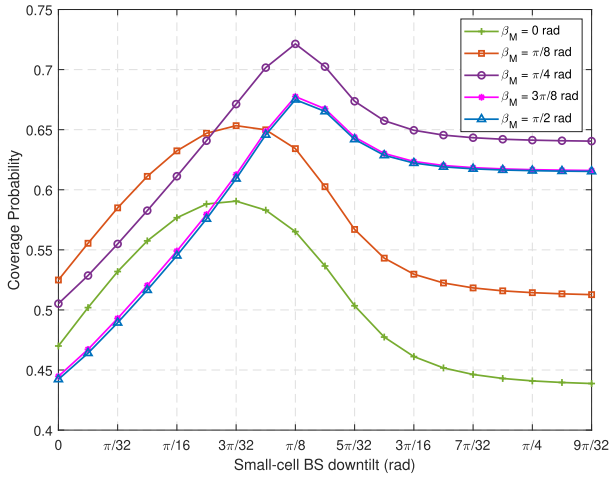

FIGURE 4. Spatially-averaged coverage probability of a two-tier HCN versus the SBS antenna downtilt for different MBS antenna downtilts.

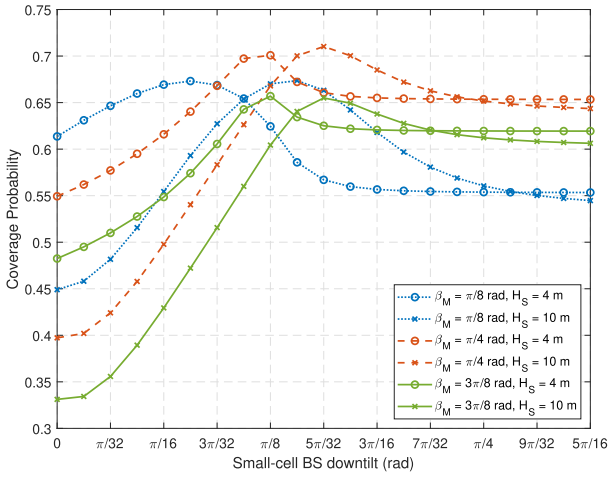

FIGURE 5. Spatially-averaged coverage probability of a two-tier HCN versus the SBS antenna downtilt for different SBS heights and MBS antenna downtilts.

versus the small-cell association bias at $\beta_M = \frac{\pi}{4}$ rad and $\beta_S = \frac{\pi}{16}, \frac{\pi}{8}, \frac{\pi}{4}$ rad, respectively. Each group of curves are shown with the same colour and marker for a β_S setting. For each β_S considered, as small-cell association bias B_S rises, the coverage probability of the macro-cell tier increases and that of the small-cell tier decreases because users at the small-cell edge are transformed into macro-cell tier users, which results in the fact that the coverage probability for the whole HCN first goes up then drops down after reaching a maximum value. For each B_S considered, increasing β_S leads to the increase of macro-cell tier coverage probability, while the coverage probability of small-cell tier first increases then decreases. The maximum coverage probability of the whole HCN achieves a much larger value at $\beta_S = \frac{\pi}{8}$ rad than that at other β_S. Since P_M is larger than P_S, MBSs can offer stronger received signal to increase the SIR of cell-edge users, which enables the enhancement in the coverage probability of macro-cell tier, while weakening that of small-cell tier to realize the traffic offloading from small-cell tier to macro-cell tier. In result, an appropriate B_S can balance the load of a HCN and maximize the overall coverage probability for a given pair of β_M and β_S. For a given B_S, increasing β_S mitigates interference from the small-cell tier to MBS users, which improves the coverage probability of macro-cell tier. However, the coverage probability of small-cell tier decreases when beams from SBSs are close to the small-cell edge or small-cell centre.

Fig. 4 presents the spatially-averaged coverage probability in terms of β_S with $B_S = 5$ dB for different β_M from 0 to $\frac{\pi}{2}$ rad. We observe that for each β_M, the coverage probability first rises with β_S then declines after reaching a maximum value. The maximum coverage probability increases with the growth of β_M and achieves the largest value when β_M is around $\frac{\pi}{4}$ rad, then decreases and does not have a significant change in the large downtilt range. In general, small downtilts lead to much interference due to the overlapping among beams. As MBSs are higher than SBSs, the traffic for small-cell tier is offloaded to macro-cell tier when the biased association is applied. In this case, MBSs have larger coverage area than that in the unbiased association scheme, hence the optimal β_M is shown in the middle of the downtilt range. In addition, although large downtilts provide enough protection against the interference, most of users cannot receive sufficient desired power due to the small antenna gain.

In Fig.5, we investigate the relationship between β_S and H_S with $B_S = 5$ dB at $\beta_M = \frac{\pi}{8}, \frac{\pi}{4}, \frac{3\pi}{8}$ rad, respectively. For each case, the coverage probability first goes up with the β_S then starts to drop after reaching a maximum value. For each H_S considered, the maximum coverage probability first increases then decreases with the increase of β_M. For each β_M considered, we observe that the optimal β_S of taller SBSs is always larger than that of shorter SBSs, since $\theta_S = \tan^{-1}\left(\frac{h_S}{d}\right)$ illustrates that taller SBSs require larger antenna downtilt to improve the desired signal. In addition, larger downtilt can mitigate inter-cell interference. For the small value of β_M, the value of the maximum coverage probability of $H_S = 4$ m is slightly higher than that of $H_S = 10$ m, but is outstripped by that of $H_S = 10$ m for the large value of β_M. When MBS antenna downtilt increases, a typical taller SBS user can suffer less interference from MBSs, whereas interfering beams are easier to point the area closes to a typical shorter SBS user.

In Fig. 6, we consider the effect of β_S and λ_S on the spatially-averaged coverage probability with $B_S = 0$ dB and $\beta_M = \frac{\pi}{4}$ rad. It can be seen that the coverage probability decreases monotonically when $\beta_S < \frac{\pi}{16}$ rad; when $\beta_S > \frac{\pi}{16}$ rad, the coverage probability first goes up then goes down after reaching a maximum value. In addition, the value of the maximum coverage probability increases with the increase of β_S, since massive SBSs leads to the growth of small-cell tier association probability and the shrinkage of coverage area of each SBS. β_S rises to avoid beam overlapping and meet the demand of high SIR for cell centre users. We also

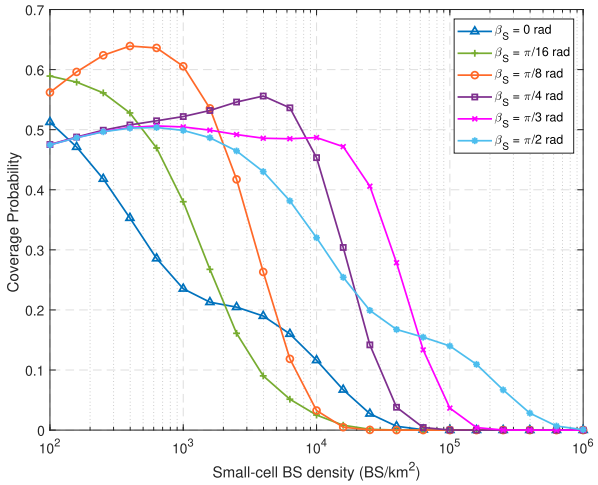

FIGURE 6. Spatially-averaged coverage probability of a two-tier HCN versus the small-cell BS density for different SBS antenna downtilts at $\beta_M = \frac{\pi}{4}$ rad.

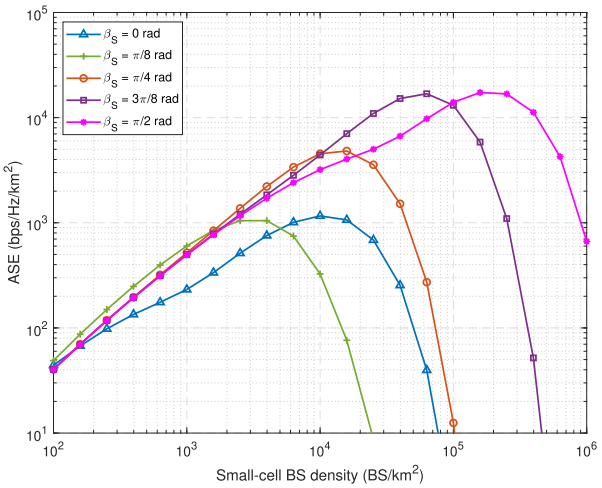

FIGURE 7. ASE of a two-tier HCN versus the small-cell BS density for different SBS antenna downtilts at $\beta_M = \frac{\pi}{4}$ rad.

observe that when the SBS antenna downtilt tends to $\frac{\pi}{2}$, there are two peaks on the curves. The first peak is much larger than the second peak because large β_S cannot supply adequate signals to SBS users. Small λ_S results in more users being associated with MBSs, which increases the coverage probability of macro-cell tier.

From (30), the ASE versus λ_S with $B_S = 0$ dB for different β_S are presented in Fig. 7. It is shown that as β_S increases, the ASE ratchets up first then declines drastically after reaching a maximum value. The maximum ASE and the corresponding λ_S both boost as the β_S rises.

C. THE OPTIMAL DOWNTILT PAIR

In this subsection, we obtain the optimal MBS and SBS antenna downtilt pair with different SBS heights and SBS densities. The uniqueness and type of the solution to (32) is analysed as well. The spatially-averaged coverage probability with the optimal MBS and SBS antenna downtilt pair is

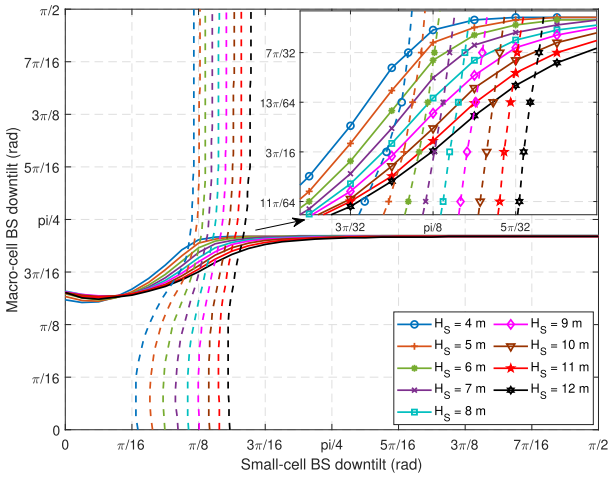

FIGURE 8. Solutions to two equations in (32) for different SBS heights by holding β_S and β_M in the range of $\left[0, \frac{\pi}{2}\right]$, respectively.

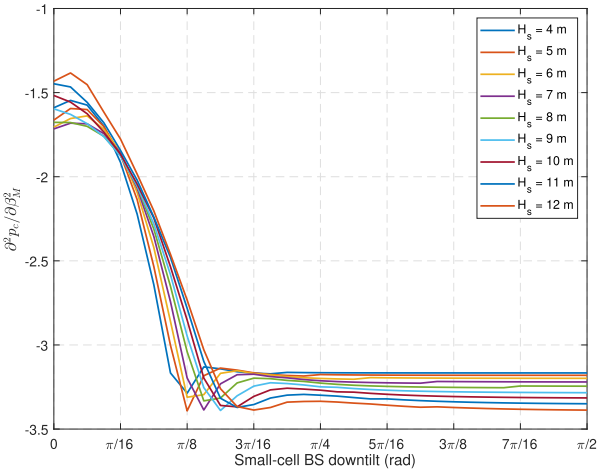

FIGURE 9. Second derivative test results of (49) for different SBS heights.

compared to that with a pair of fixed MBS and SBS antenna downtilts.

Fig.8 shows solutions to two equations in (32) for different SBS heights, where solid lines and dashed lines are solutions to $\mathcal{A}_M \frac{\partial \mathcal{P}_M}{\partial \beta_M} + \mathcal{A}_S \frac{\partial \mathcal{P}_S}{\partial \beta_M} = 0$ for $\beta_S \in \left[0, \frac{\pi}{2}\right]$ and $\mathcal{A}_M \frac{\partial \mathcal{P}_M}{\partial \beta_S} + \mathcal{A}_S \frac{\partial \mathcal{P}_S}{\partial \beta_S} = 0$ for $\beta_M \in \left[0, \frac{\pi}{2}\right]$, respectively. The intersection of the solid line and the dashed line for each H_S represents the stationary point (β_M^*, β_S^*). It is obviously that there is only one intersection for each H_S, which proves the uniqueness of (β_M^*, β_S^*). Fig.9 and Fig.10 present results of (49) and (50), respectively. As all results are below 0, we can ensure that (β_M^*, β_S^*) is the unique maximum point for a given H_S.

Fig. 11 shows the optimal MBS antenna downtilt and SBS antenna downtilt obtained via the stationary points for different H_S and λ_S. There are some error between analysis and simulation due to the sampling intervals in Algorithm 1 and the simulation. Since the coverage probability at the optimal MBS and SBS antenna downtilt pair and that at the adjacent pair have negligible difference, these error are acceptable.

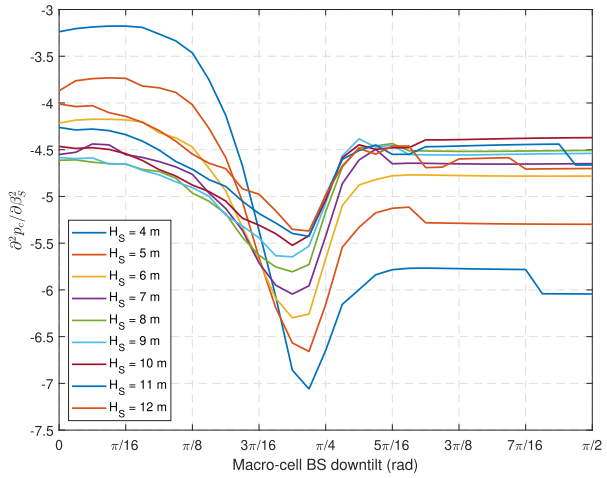

FIGURE 10. Second derivative test results of (50) for different SBS heights.

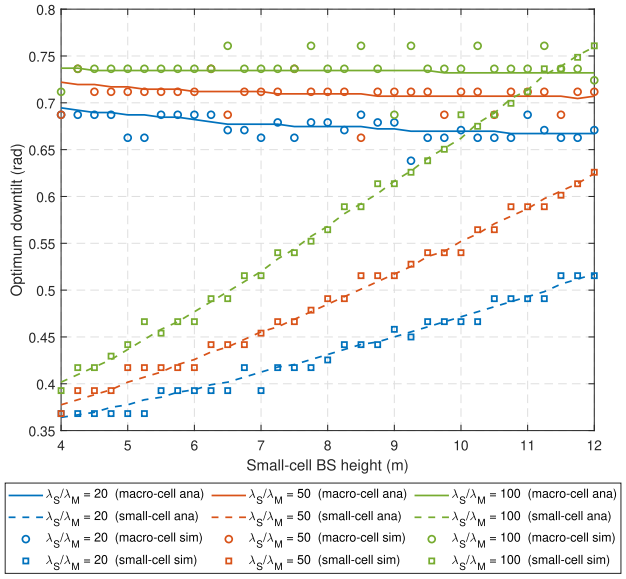

FIGURE 11. The optimal MBS antenna downtilt and SBS antenna downtilt versus the SBS height for different small-cell BS densities in analysis and simulation, respectively.

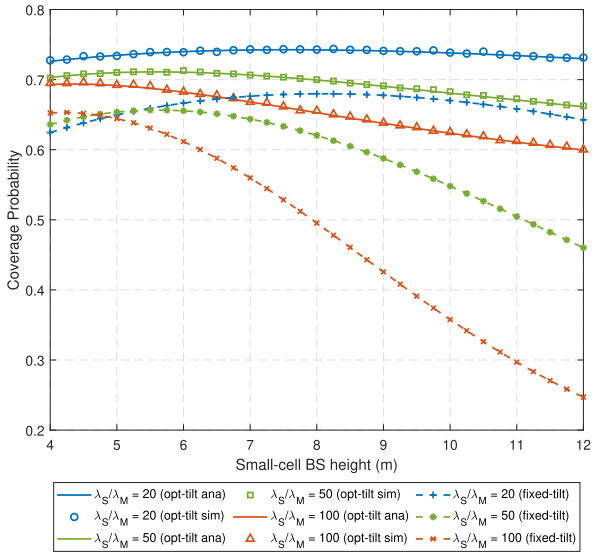

FIGURE 12. Comparison of the spatially-averaged coverage probability with or without the optimal pair of MBS and SBS antenna downtilts versus the SBS height for different SBS densities in analysis and simulation, respectively.

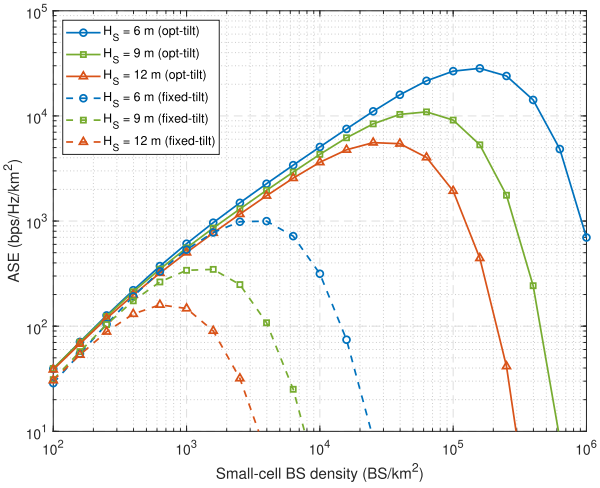

FIGURE 13. Comparison of ASE with or without the optimal pair of MBS and SBS antenna downtilts versus the SBS density for different SBS heights.

For each λ_S considered, the optimal SBS antenna downtilt grows monotonically as H_S increases to reduce interference in the small-cell tier. The optimal MBS antenna downtilt decreases quite slightly, which illustrates that it is not strongly affected by H_S. For each H_S considered, deploying more SBSs increases both optimal MBS antenna downtilt and SBS antenna downtilt to enhance signals and reduce inter-cell interference due to the overlap among beams in both tiers.

Fig. 12 represents the spatially-averaged coverage probability with the corresponding optimal MBS and SBS antenna downtilts for varying H_S and λ_S in analysis and simulation, respectively. It is exhibited that for each H_S considered, increasing λ_S degrades the coverage probability. Although all coverage probabilities are obtained when the optimal pair of MBS and SBS antenna downtilts are applied, adding redundant SBSs still increases beams overlapping to MBSs because of the reduction of MBS association probability. This can also explain why dense small-cell tier requires lower SBSs in this figure. For each H_S and λ_S considered, the HCN with the optimal pair of MBS and SBS antenna downtilts significantly improve the downlink coverage probability.

Fig. 13 plots the ASE with the optimal MBS antenna downtilt and SBS antenna downtilt and that with the fixed MBS antenna downtilt and SBS antenna downtilt versus the λ_S for different H_S. It can be seen that for each case, the ASE first increases with λ_S and then starts to decrease after reaching a maximum value. For each H_S considered, the optimal pair of MBS and SBS antenna downtilts achieve a much larger value of the maximum ASE at a higher λ_S than the case without optimizing the BS antenna downtilts. For each H_S and λ_S

considered, the HCN with the optimal pair of MBS and SBS antenna downtilts brings about a significant ASE enhancement. With or without optimizing the BS antenna downtilts, for the same λ_S, the ASE decreases with the increase of H_S.

VI. CONCLUSION

In this paper, we proposed a two-tier HCN with stochastic geometry framework to analyze the downlink spatially-averaged coverage probability and ASE when considering the antenna downtilts in both tiers as optimization parameters. To facilitate the computation efficiency, we leverage the Gauss-Chebyshv quadrature method for approximating integral parts in Laplace transforms. Results indicate that adjusting BS antenna downtilts in both tiers has a significant impact on the spatially-averaged coverage probability and ASE of HCNs. Under the minimum biased transmission distance user association scheme, the SBS antenna height, SBS association bias and SBS density can determine the optimal BS antenna downtilt. We then derive the optimal MBS antenna downtilt and SBS antenna downtilt to maximize the spatially-averaged coverage probability and ASE. Results lead to the conclusion that the optimal SBS antenna downtilt increases as the height of SBS rises to alleviate the inter-cell interference, while MBS antenna downtilt does not have significantly change. Moreover, the SBS height and the SBS density still have impact on the spatially-averaged coverage probability and ASE on condition that antenna downtilts in both tiers are optimal. The presented model shows that the MBS antenna downtilt and SBS antenna downtilt can be adapted effectively to improve the performance of HCNs in terms of the spatially-averaged coverage probability and ASE. We will design line-of-sight/non-line-of-sight transmission and consider Nakagami fading in our future work.

APPENDIX A COVERAGE PROBABILITY

$\Pr\left[\mathrm{SIR}_i^M > \tau\right]$ in (17) is derived as

$$\begin{aligned}
&\Pr\left[\mathrm{SIR}_i^M > \tau\right] \\
&= \Pr\left[\frac{g_i^M P_M L_i^M G_i^M}{I_i^M + I_M^S} > \tau\right] \\
&= \Pr\left[g_i^M > \tau \frac{I_i^M + I_M^S}{P_M L_i^M G_i^M}\right] \\
&= \mathbb{E}_{I_i^M, I_M^S}\left[\Pr\left(g_i^M > \frac{\tau\left(I_i^M + I_M^S\right)}{P_M L_i^M G_i^M}\right)\right] \\
&\overset{(c)}{=} \mathbb{E}_{I_i^M, I_M^S}\left[\exp\left(-\tau \frac{I_i^M + I_M^S}{P_M L_i^M G_i^M}\right)\right] \\
&= \mathcal{L}_{I_i^M}\mathcal{L}_{I_M^S}, \qquad (59)
\end{aligned}$$

where (c) follows $g_i^M \sim \exp(1)$. Utilizing the definition of Laplace transform yields, $\mathcal{L}_{I_i^M}$ and $\mathcal{L}_{I_M^S}$ can be calculated as

$$\begin{aligned}
\mathcal{L}_{I_i^M} &= \mathbb{E}_{I_M}\left[e^{-\frac{\tau}{P_M L_i^M G_i^M} I_i^M}\right] \\
&= \mathbb{E}_{\Phi'_M}\left[\exp\left(-\frac{\tau}{P_M L_i^M G_i^M} \sum_{k \in \Phi'_M \setminus \{i\}} g_k^M P_M L_k^M G_k^M\right)\right] \\
&\overset{(d)}{=} \exp\left[\frac{-2\pi\lambda_M}{s} \int_x^\infty \left\{1 - \mathcal{L}_{g_M}\left(\frac{\tau L_k^M G_k^M}{L_i^M G_i^M}\right)\right\} d_k^M \mathrm{d}d_k^M\right] \\
&= \exp\left[\frac{-2\pi\lambda_M}{s} \int_x^\infty \frac{d_k^M}{1 + \mathcal{K}_i^M \frac{G_i^M}{G_k^M}} \mathrm{d}d_k^M\right], \qquad (60) \\
\mathcal{L}_{I_M^S} &= \mathbb{E}_{I_M}\left[e^{-\frac{\tau}{P_M L_i^M G_i^M} I_M^S}\right] \\
&= \mathbb{E}_{\Phi_S}\left[\exp\left(-\frac{\tau}{P_M L_i^M G_i^M} \sum_{l \in \Phi_S} g_l^M P_S L_l^M G_j^M\right)\right] \\
&= \exp\left[-2\pi\lambda_S \int_{W_M}^\infty \left\{1 - \mathcal{L}_{g_S}\left(\frac{\tau P_S L_l^M G_l^M}{P_M L_i^M G_i^M}\right)\right\} d_l^M \mathrm{d}d_l^M\right] \\
&= \exp\left[-2\pi\lambda_S \int_{W_M}^\infty \frac{d_l^M}{1 + \mathcal{K}_M^S \frac{G_i^M}{G_l^M}} \mathrm{d}d_l^M\right], \qquad (61)
\end{aligned}$$

where (d) follows from the probability generating functional of the PPP [32]. Since the serving MBS is the nearest MBS in the shortest biased transmission distance cell-association scheme, according to (12), W_M is given by (20).

Let t represent the tier index that the typical user is associated with. When the typical user is associated with the macro-cell tier, the PDF of d_i^M is expressed as

$$\begin{aligned}
f_{d_i^M}(x) &= \frac{\mathrm{d}\left\{\Pr\left[x < d_i^M\right]\right\}}{\mathrm{d}x} \\
&= \frac{\Pr\left[x < d_M, t = M\right]}{\Pr[t = M] \cdot \mathrm{d}x}, \qquad (62)
\end{aligned}$$

where $\Pr[t = M] = \mathcal{A}_M$ follows from the definition of $\mathcal{A}_M$, and

$$\begin{aligned}
&\Pr\left[x < d_M, t = M\right] \\
&= \int_x^\infty \Pr\left[D_M < D_S\right] f_{d_M}(r)\, \mathrm{d}r. \qquad (63)
\end{aligned}$$

Inserting (63) into (62), the PDF of d_i^M can be rewritten as (21). The proof is completed.

REFERENCES

[1] A. Damnjanovic, J. Montojo, Y. Wei, T. Ji, T. Luo, M. Vajapeyam, T. Yoo, O. Song, and D. Malladi, "A survey on 3GPP heterogeneous networks," *IEEE Wireless Commun.*, vol. 18, no. 3, pp. 10–21, Jun. 2011.
[2] J. G. Andrews, S. Buzzi, W. Choi, S. V. Hanly, A. Lozano, A. C. K. Soong, and J. C. Zhang, "What will 5G be?" *IEEE J. Sel. Areas Commun.*, vol. 32, no. 6, pp. 1065–1082, Jun. 2014.
[3] A. Ghosh, N. Mangalvedhe, R. Ratasuk, B. Mondal, M. Cudak, E. Visotsky, T. A. Thomas, J. G. Andrews, P. Xia, H. S. Jo, H. S. Dhillon, and T. D. Novlan, "Heterogeneous cellular network: From theory to practice," *IEEE Commun. Mag.*, vol. 50, no. 6, pp. 54–64, Jun. 2012.
[4] R. W. Heath, Jr., M. Kountouris, and T. Bai, "Modeling heterogeneous network interference using Poisson point processes," *IEEE Trans. Signal Process.*, vol. 61, no. 16, pp. 4114–4126, Aug. 2013.
[5] H.-S. Jo, Y. J. Sang, P. Xia, and J. G. Andrews, "Heterogeneous cellular networks with flexible cell association: A comprehensive downlink SINR analysis," *IEEE Trans. Wireless Commun.*, vol. 11, no. 10, pp. 3484–3494, Oct. 2012.

[6] H. S. Dhillon, R. K. Ganti, F. Baccelli, and J. G. Andrews, "Modeling and analysis of K-tier downlink heterogeneous cellular networks," *IEEE J. Sel. Areas Commun.*, vol. 30, no. 3, pp. 550–560, Apr. 2012.
[7] J. Wang, X. Chu, M. Ding, and D. Lopez-Perez, "On the performance of multi-tier heterogeneous networks under LoS and NLoS transmissions," in *Proc. IEEE Globecom Workshops (GC Wkshps)*, Dec. 2016, p. 5.
[8] H. Hu, J. Zhang, X. Chu, and J. Zhang, "Downlink coverage analysis of K-Tier heterogeneous networks with multiple antennas," in *Proc. IEEE Int. Conf. Commun. (ICC)*, May 2019, pp. 1–6.
[9] C. Chen, J. Zhang, X. Chu, and J. Zhang, "On the optimal base-station height in mmWave small-cell networks considering cylindrical blockage effects," *IEEE Trans. Veh. Technol.*, vol. 70, no. 9, pp. 9588–9592, Sep. 2021.
[10] Q.-U.-A. Nadeem, A. Kammoun, and M.-S. Alouini, "Elevation beamforming with full dimension MIMO architectures in 5G systems: A tutorial," *IEEE Commun. Surveys Tuts.*, vol. 21, no. 4, pp. 3238–3273, 4th Quart., 2019.
[11] S. M. Razavizadeh, M. Ahn, and I. Lee, "Three-dimensional beamforming: A new enabling technology for 5G wireless networks," *IEEE Signal Process. Mag.*, vol. 31, no. 6, pp. 94–101, Nov. 2014.
[12] J. G. Andrews, F. Baccelli, and R. K. Ganti, "A tractable approach to coverage and rate in cellular networks," *IEEE Trans. Commun.*, vol. 59, no. 11, pp. 3122–3134, Oct. 2011.
[13] D. Liu, L. Wang, Y. Chen, M. Elkashlan, K. Wong, R. Schober, and L. Hanzo, "User association in 5G networks: A survey and an outlook," *IEEE Commun. Surveys Tuts.*, vol. 18, no. 2, pp. 1018–1044, 2nd Quart., 2016.
[14] S. Singh, H. S. Dhillon, and J. G. Andrews, "Offloading in heterogeneous networks: Modeling, analysis, and design insights," *IEEE Trans. Wireless Commun.*, vol. 12, no. 5, pp. 2484–2497, May 2013.
[15] A. K. Gupta, H. S. Dhillon, S. Vishwanath, and J. G. Andrews, "Downlink multi-antenna heterogeneous cellular network with load balancing," *IEEE Trans. Commun.*, vol. 62, no. 11, pp. 4052–4067, Nov. 2014.
[16] C. Chen, J. Zhang, X. Chu, and J. Zhang, "On the deployment of small cells in 3D HetNets with multi-antenna base stations," *IEEE Trans. Wireless Commun.*, vol. 21, no. 11, pp. 9761–9774, Nov. 2022, doi: 10.1109/TWC.2022.3179283.
[17] E. Turgut and M. C. Gursoy, "Coverage in heterogeneous downlink millimeter wave cellular networks," *IEEE Trans. Commun.*, vol. 65, no. 10, pp. 4463–4477, Oct. 2017.
[18] E. Mugume and D. K. C. So, "User association in energy-aware dense heterogeneous cellular networks," *IEEE Trans. Wireless Commun.*, vol. 16, no. 3, pp. 1713–1726, Mar. 2017.
[19] Y. S. Soh, T. Q. S. Quek, M. Kountouris, and H. Shin, "Energy efficient heterogeneous cellular networks," *IEEE J. Sel. Areas Commun.*, vol. 31, no. 5, pp. 840–850, May 2013.
[20] M. Tang, G. Cui, X. Zou, W. Wang, and Y. Zhang, "A 3D-beamforming scheme for throughput optimization in heterogeneous network," in *Proc. IEEE Int. Conf. Cloud Comput. Intell. Syst.*, Nov. 2014, pp. 222–227.
[21] X. Li, C. Li, S. Jin, and X. Gao, "Interference coordination for 3-D beamforming-based HetNet exploiting statistical channel-state information," *IEEE Trans. Wireless Commun.*, vol. 17, no. 10, pp. 6887–6900, Oct. 2018.
[22] D. Li, J. Xu, X. Wang, and X. Tao, "Joint optimization for cell association and vertical downtilts adjustment in 3D MIMO enabled HetNets," in *Proc. IEEE Wireless Commun. Netw. Conf. (WCNC)*, Apr. 2018, pp. 1–6.
[23] X. Li, T. Bai, and R. W. Heath, Jr., "Impact of 3D base station antenna in random heterogeneous cellular networks," in *Proc. IEEE Wireless Commun. Netw. Conf. (WCNC)*, Apr. 2014, pp. 2254–2259.
[24] X. Li, R. W. Heath, Jr., K. Linehan, and R. Butler, "Impact of metro cell antenna pattern and downtilt in heterogeneous networks," 2015, *arXiv:1502.05782*.
[25] R. Hernandez-Aquino, S. A. R. Zaidi, D. McLernon, M. Ghogho, and A. Imran, "Tilt angle optimization in two-tier cellular networks—A stochastic geometry approach," *IEEE Trans. Commun.*, vol. 63, no. 12, pp. 5162–5177, Dec. 2015.
[26] E. Mugume, "Green heterogeneous cellular networks," Ph.D. Dissertation, Faculty Eng. Phys. Sci., Univ. Manchester, Manchester, U.K., 2016.
[27] *Study 3D Channel Model for LTE (Release12)*, document TR 36.873, V12.7.0, 3GPP, Technical Specification, Group Radio, and Access Network, Dec. 2017.
[28] F. Gunnarsson, M. N. Johansson, A. Furuskar, M. Lundevall, A. Simonsson, C. Tidestav, and M. Blomgren, "Downtilted base station antennas—A simulation model proposal and impact on HSPA and LTE performance," in *Proc. IEEE 68th Veh. Technol. Conf.*, Sep. 2008, pp. 1–5.
[29] D. López-Pérez, M. Ding, H. Claussen, and A. H. Jafari, "Towards 1 Gbps/UE in cellular systems: Understanding ultra-dense small cell deployments," *IEEE Commun. Surveys Tuts.*, vol. 17, no. 4, pp. 2078–2101, 4th Quart., 2015.
[30] C. A. Balanis, *Antenna Theory: Analysis and Design*, Hoboken, NJ, USA: Wiley, 2005.
[31] T. Bai and R. W. Heath, "Coverage and rate analysis for millimeter-wave cellular networks," *IEEE Trans. Wireless Commun.*, vol. 14, no. 2, pp. 1100–1114, Feb. 2015.
[32] R. L. Streit, *Poisson Point Processes: Imaging, Tracking, and Sensing*. New York, NY, USA: Springer, 2010.
[33] M. Abramowitz and I. A. Stegun, *Handbook of Mathematical Functions With Formulas, Graphs, and Mathematical Tables*. New York, NY, USA: Dover, 1972.
[34] M.-S. Alouini and A. J. Goldsmith, "Area spectral efficiency of cellular mobile radio systems," *IEEE Trans. Veh. Technol.*, vol. 48, no. 4, pp. 1047–1066, Jul. 1999.
[35] C. Li, J. Zhang, J. G. Andrews, and K. B. Letaief, "Success probability and area spectral efficiency in multiuser MIMO HetNets," *IEEE Trans. Commun.*, vol. 64, no. 4, pp. 1544–1556, Apr. 2016.
[36] G. F. Simmons, *Calculus With Analytic Geometry*, 2nd ed. New York, NY, USA: McGraw-Hill, 1995.
[37] S. L. Grossman, *Calculus*, 3rd ed. Amsterdam, The Netherlands: Elsevier, 1984.

MENGXIN ZHOU received the B.Eng. degree in electronic and communication engineering from The University of Sheffield, Sheffield, U.K., in 2017, where she is currently pursuing the Ph.D. degree. Her research interests include massive MIMO techniques, millimeter-wave networks, heterogeneous networks, and stochastic geometry.

CHEN CHEN (Member, IEEE) received the B.E. degree from the East China University of Science and Technology, in 2018, and the Ph.D. degree from The University of Sheffield, in 2022. Since January 2022, he has been a Postdoctoral Research Assistant at the University of Liverpool. His current research interests include millimeter wave networks, massive MIMO, wireless security, stochastic geometry, and machine learning.

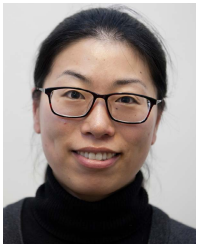

XIAOLI CHU (Senior Member, IEEE) received the B.Eng. degree in electronic and information engineering from Xi'an Jiao Tong University, in 2001, and the Ph.D. degree in electrical and electronic engineering from The Hong Kong University of Science and Technology, in 2005. She is currently a Professor with the Department of Electronic and Electrical Engineering, The University of Sheffield, U.K. From 2005 to 2012, she was with the Centre for Telecommunications Research, King's College London. She has coauthored over 160 peer-reviewed journals and conference papers. She was a co-recipient of the IEEE Communications Society 2017 Young Author Best Paper Award. She coauthored/co-edited the books *Fog-Enabled Intelligent IoT Systems* (Springer, 2020), *Ultra Dense Networks for 5G and Beyond* (Wiley, 2019), *Heterogeneous Cellular Networks—Theory, Simulation and Deployment* (Cambridge University Press, 2013), and *4G Femtocells: Resource Allocation and Interference Management* (Springer, 2013). She is the Senior Editor for the IEEE Wireless Communications Letters. She was an Editor of the IEEE Communications Letters (2016–2021), and received the IEEE Communications Letters Exemplary Editor Award, in 2018. She was the Co-Chair of Wireless Communications Symposium for IEEE ICC 2015 and has co-organized eight workshops at IEEE ICC, GLOBECOM, WCNC, and PIMRC.